Article

Neuron

The Transition from Evaluation to Selection Involves Neural Subspace Reorganization in Core Reward Regions

Highlights

- Transition from evaluation to comparison is associated with subspace orthogonalization
- This orthogonalization may prevent evaluation from prematurely influencing selection
- The relative positions of encoded values remain preserved despite orthogonalization

Authors

Seng Bum Michael Yoo, Benjamin Y. Hayden

Correspondence

sbyoo.ur.bcs@gmail.com

In Brief

Economic choice proceeds from evaluation, in which we contemplate options, to selection, in which we weigh options and choose one. Yoo and Hayden show that these two stages are associated with orthogonalized subspaces. This orthogonalization may help keep two processes taking place in the same area from interfering.

Yoo & Hayden, 2020, Neuron *105*, 1–13
February 19, 2020
https://doi.org/10.1016/j.neuron.2019.11.013

CellPress

Please cite this article in press as: Yoo and Hayden, The Transition from Evaluation to Selection Involves Neural Subspace Reorganization in Core Reward Regions, Neuron (2019), https://doi.org/10.1016/j.neuron.2019.11.013

Neuron
Article

CellPress

The Transition from Evaluation to Selection Involves Neural Subspace Reorganization in Core Reward Regions

Seng Bum Michael Yoo[1,2,*] and Benjamin Y. Hayden[1]
[1]Department of Neuroscience, Center for Magnetic Resonance Research, Center for Neuroengineering, University of Minnesota, Minneapolis, MN 55455, USA
[2]Lead Contact
*Correspondence: sbyoo.ur.bcs@gmail.com
https://doi.org/10.1016/j.neuron.2019.11.013

SUMMARY

Economic choice proceeds from evaluation, in which we contemplate options, to selection, in which we weigh options and choose one. These stages must be differentiated so that decision makers do not proceed to selection before evaluation is complete. We examined responses of neurons in two core reward regions, orbitofrontal (OFC) and ventromedial prefrontal cortex (vmPFC), during two-option choice with asynchronous offer presentation. Our data suggest that neurons selective during the first (presumed evaluation) and second (presumed comparison and selection) offer epochs come from a single pool. Stage transition is accompanied by a shift toward orthogonality in the low-dimensional population response manifold. Nonetheless, the relative position of each option in driving responses in the population subspace is preserved. The orthogonalization we observe supports the hypothesis that the transition from evaluation to selection leads to reorganization of response subspace and suggests a mechanism by which value-related signals are prevented from prematurely driving choice.

INTRODUCTION

Imagine a cheetah patiently scanning a herd of Thomson's gazelles to identify one to chase. The cheetah must first evaluate all its options before selecting one and initiating pursuit (Cooper et al., 2007). The cheetah is facing a control problem faced by many decision makers. It must separate evaluation—in which the subject deliberates over available options—from selection—in which options are weighed and a preferred one is chosen (Levy and Glimcher, 2012; Montague and Berns, 2002; Padoa-Schioppa, 2011; Padoa-Schioppa et al., 2006; Rangel et al., 2008; Sigman and Dehaene, 2005; Thura and Cisek, 2014). Failing to separate them, the cheetah would be at risk of selecting the first encountered reasonable option and could never move past a good one to obtain the best available one. More generally, the brains of decision makers must keep evaluation and selection stages cleanly separated so that evaluation can be done sufficiently well before selection begins.

How does the brain separate stages during economic choice? One possibility would be to have stages associated with anatomically different brain structures or, equivalently, with distinct sets of neurons in a single structure (e.g., Chau et al., 2014; Chen and Stuphorn, 2015; Padoa-Schioppa and Cai, 2011; Rustichini and Padoa-Schioppa, 2015; Wunderlich et al., 2010). In this way, activation of choice-related neurons could easily be gated until evaluation neurons reach a consensus. This possibility appears inconsistent with at least some data—brain regions and neurons associated with evaluation are generally associated with comparison and vice versa (e.g., Azab and Hayden, 2017; Cisek, 2012; Hunt et al., 2012, 2014; Noonan et al., 2012). This is particularly true in the two most commonly identified reward regions, orbitofrontal cortex (OFC) and ventromedial prefrontal cortex (vmPFC). Both areas are closely associated with evaluation and comparison (Bartra et al., 2013; Levy and Glimcher, 2012; Noonan et al., 2010; Padoa-Schioppa, 2011; Strait et al., 2014; Wallis, 2007).

Another way for the brain to gate deliberations from triggering action is to use a thresholding procedure (Gold and Shadlen, 2007; Kacelnik et al., 2011; Krajbich et al., 2010; Polanía et al., 2014; Shadlen and Shohamy, 2016; Thura et al., 2012). That is, neurons could perform qualitatively the same type of computations that drive action but do those computations in a subthreshold (lower firing rate or firing rate variance) manner that is sufficient to compute but insufficient to trigger action. The gating then would happen on two sides of a single critical threshold firing rate. The thresholding idea has proven to be attractive in neuroeconomics and is supported by at least some evidence in a variety of choice contexts (Hayden et al., 2011; Krajbich and Rangel, 2011; Krajbich et al., 2010; Polanía et al., 2019; Shadlen and Shohamy, 2016; Tajima et al., 2016; Blanchard et al., 2015).

Recent evidence argues against the idea that thresholds distinguish motor preparatory from executive activity, suggesting that the corresponding elements of economic choice—evaluation and selection—may also not rely, at least solely, on thresholding either (Elsayed et al., 2016; Kaufman et al., 2014). Specifically, there is no evidence that preparatory activity is of lower amplitude than executive activity. Echoing these motor

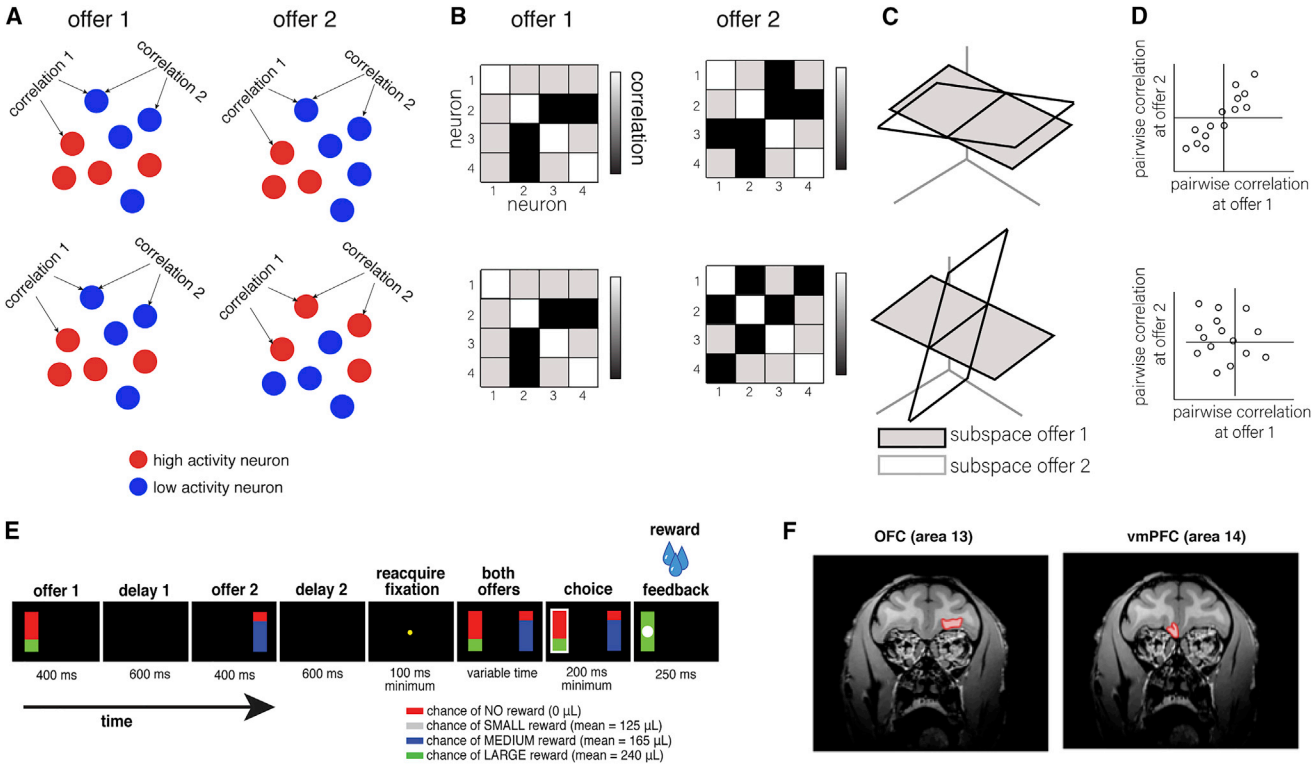

Figure 1. General Ideas and Methods

(A–D) Top row: schematic for subspace preservation; bottom row: schematics for subspace orthogonalization.

(A) Cartoon showing activity of neurons in an ensemble; correlation is computed on each pair of neurons. When subspaces orthogonalize (bottom row), the mathematical relationship limiting correlations of neuron papers is disrupted.

(B) During subspace orthogonalization, the change in subspace is visible in the form of a large change in the correlation matrix.

(C) The subspace is indicated by a plane in a larger space. This view makes it clear that subspace orthogonalization consists of a rotation.

(D) A key signature of subspace orthogonalization is a reduction in the correlation of correlation points for each individual pair of neurons.

(E) The task structure of sequential gambling task (Strait et al., 2014). The stakes and probability of each option are selected randomly each trial. In the example trial, the second offer has higher offer value.

(F) MRI image for two subjects for the recorded brain areas: area 13 (OFC) and area 14 (vmPFC).

results, we find no systematic rise in activity moving from putative evaluation to executive periods, even when this activity shows clear signatures of transition from evaluation to comparison-related activity (Azab and Hayden, 2017; Strait et al., 2014).

A third mechanism for gating is a change in neuronal ensemble codes, such as a rotation to a null subspace or a change in population subspace occupancy from one epoch to the next (Churchland et al., 2010; Crammond and Kalaska, 2000; Elsayed et al., 2016; Johnson et al., 1999; Kaufman et al., 2014; Stavisky et al., 2017). If the tuning structure rotates orthogonally as the decision maker moves from one stage to the next, then evaluation-related computations occurring in the evaluation subspace will cancel out when projected onto output-potent dimensions. Following the completion of evaluation, a subspace rotation could enable the responses to drive downstream—or perhaps local—activity and promote selection (Figure 1A). Although this idea has not (as far as we know) been proposed in the domain of economic choice, it is consistent with proposals in motor and oculomotor domains (Hannah et al., 2018; Kaufman et al., 2014; Khanna et al., 2019; Stavisky et al., 2017).

Of these approaches, the most well supported is the idea that gating occurs through a "subspace rotation" (Elsayed et al., 2016). During the evaluation phase of the task, for each pair of neurons, there is a lawful mathematical relationship that restricts the way their joint responses can covary. In other words, for any pair of neurons, there exists a covariance function that describes limits imposed on the firing of one neuron given the firing of the other. The set of all such relationships, for all neuron pairs in a population, defines the manifold along which the ensemble firing rate pattern can travel. When transitioning from movement preparation to execution, neuronal ensembles in motor cortex change covariance subspaces but maintain relative motor tuning, preventing motor preparation from triggering premature action (Elsayed et al., 2016). In other words, control of function can be accomplished even if the relative tuning of individual neuron remains the same. This is important given evidence for preserved tuning across ostensible evaluation and selection epochs in vmPFC, OFC, and other core reward regions (Azab and Hayden, 2018; Strait et al., 2014, 2015).

We examined responses of neurons in two core reward regions, area 13 of OFC and area 14 of vmPFC. The importance of OFC and area 13 to evaluation and comparison is well established (Murray et al., 2007; Padoa-Schioppa, 2011; Padoa-Schioppa and Conen, 2017; Rushworth et al., 2011; Schuck et al., 2016; Wallis, 2007; Wilson et al., 2014). The importance of the vmPFC is likewise clearly demonstrated (Bartra et al., 2013; Hare et al., 2009; Meder et al., 2017; Papageorgiou et al., 2017; Rushworth et al., 2011). Area 14 is a central element of Price's ventromedial network (Ongür and Price, 2000), which is largely synonymous with vmPFC, and area 14 appears to have structural and functional homology with core reward subregions in vmPFC and to contribute directly to evaluation and comparison (Mars et al., 2016; Rich and Wallis, 2014, 2016; Strait et al., 2014; Watson and Platt, 2012).

Macaque subjects performed a simple risky choice task with asynchronous presentation of two options. The asynchrony allowed us to temporally differentiate putative evaluation and selection phases of the task (Azab and Hayden, 2017; Strait et al., 2014, 2015). We find that, when moving from the first to the second epoch, the same populations of neurons are involved and that their population tuning function for value is preserved. At the same time, the subspace of the larger manifold occupied by the neurons rotates to become nearly orthogonal. This change allows the population to perform distinct computations with the same elements during the two epochs, thus allowing the brain to perform choice-relevant evaluation processes, but not prematurely trigger a decision. These observations support the hypothesis that there is a strong continuity of function between economic choice and motor control and are consistent with the idea that choice and motor control are two elements of a larger sensorimotor transformation process (Yoo and Hayden, 2018; Cisek, 2012).

RESULTS

Behavior in the Sequential Gambling Task

Four rhesus macaque subjects performed a two-option gambling task (Figure 1B). Two subjects were trained on the task expressly for this study, and their data described here are new (subjects P and S; OFC dataset). The other two subjects were trained and recorded for another study and their data reanalyzed here (although some new data that did not appear earlier was added; subjects B and H; vmPFC dataset; Strait et al., 2014). In our "asynchronous gambling task," options differed on two dimensions: probability (0%–100% by 1% increments) and reward size (medium, 165 μL, or large, 240 μL) and were occasionally (12.5% of trials) riskless (100% chance of 125 mL). The probabilities and stakes for both options as well as which side the first option appeared on (that is, five trial variables) were all drawn independently and from uniform distributions on each trial.

A key element of the task was the insertion of a 1-s asynchrony between the presentation of the first and second offers. This feature ensured that the subject evaluated only the first offer during the first offer epoch and allowed subjects to compare the values of the two options during the second offer epoch. Because the two offers were independent of each other, the first option provided no information about the value of the second. Consequently, subjects could not compare their values until the appearance of the second option. On the other hand, when the second option appeared, subjects could (and almost certainly did; see Azab and Hayden, 2018; Strait et al., 2014, 2015) immediately compare their values and covertly select a preferred one (even though their preference was not expressed until another second later).

All four subjects appeared to understand the task and behaved in similar and unremarkable ways. Our two vmPFC subjects chose the offer with the higher mathematical expected value (EV) ~80% of the time (subject B: 82.76%; subject H: 80.58%) and showed behavior consistent with attending to both probability and stakes dimensions of each gamble (Strait et al., 2014; for more detail justifying subjects' understanding of this task, see our past studies of behavior in this task, especially Farashahi et al., 2018 and Hayden et al., 2010). Our OFC subjects showed qualitatively similar behavior in all respects to the vmPFC subjects. Most important, they chose the higher EV option more often (subject P: 75.42%; subject S: 76.13%).

To gain insight into the mental processes occurring during the second offer epoch, we performed an additional experiment. These results in all four subjects are new for this study, although in all cases, they were collected at the time of the physiological data. On a subset of days ($n = 7$ for subjects B and H; $n = 4$ for P and S), we collected behavioral data (no electrophysiology) in a version of the task in which the two offers were not shown again at the start of the choice period (number of trials, B: 4,013; H: 3,323; P: 1,098; S: 1,389). We found that subject's performance was not impaired by this change, indicating that they successfully maintained a representation of the value of the first offer in working memory at the time of the second one. Specifically, subjects chose the higher EV option 81.1% of the time (subject B), 82.0% of the time (subject H), 73.9% of the time (subject P), and 73.3% of the time (subject S). All of these proportions are significant ($p < 0.01$; binomial test).

Distinct Covariance Structures for the Two Epochs in Both Regions

We recorded responses of 146 neurons in area 13 of OFC (subject P: 110; subject S: 36) and 180 neurons in area 14 of vmPFC (subject B: 108; subject H: 72; 156 of these were studied in Strait et al., 2014). Our first goal was to determine whether neurons used the same representational subspaces during the two offer epochs. We first asked whether there is any basic change in the covariance structure from the first epoch to the second. Such a change is not predicted by standard "single neuron doctrine" accounts of choice, including accumulation to threshold models (e.g., Gold and Shadlen, 2007). For this analysis and all subsequent ones (unless otherwise noted), we made use of the 400-ms epoch period when the visual stimulus was on the screen (Figure 1B).

In both subjects, we found that the covariance structure changed markedly. This is clear when plotting the entries of the epoch 1 covariance matrix against the entries of the epoch 2 covariance matrix: there is little relationship between them (Figures 2A and 2D). Specifically, the correlation of each vector of pairwise correlation coefficients is almost identical to zero: vmPFC: $R^2 = 0.0165 \pm 0.002$ for subject B and $R^2 =$

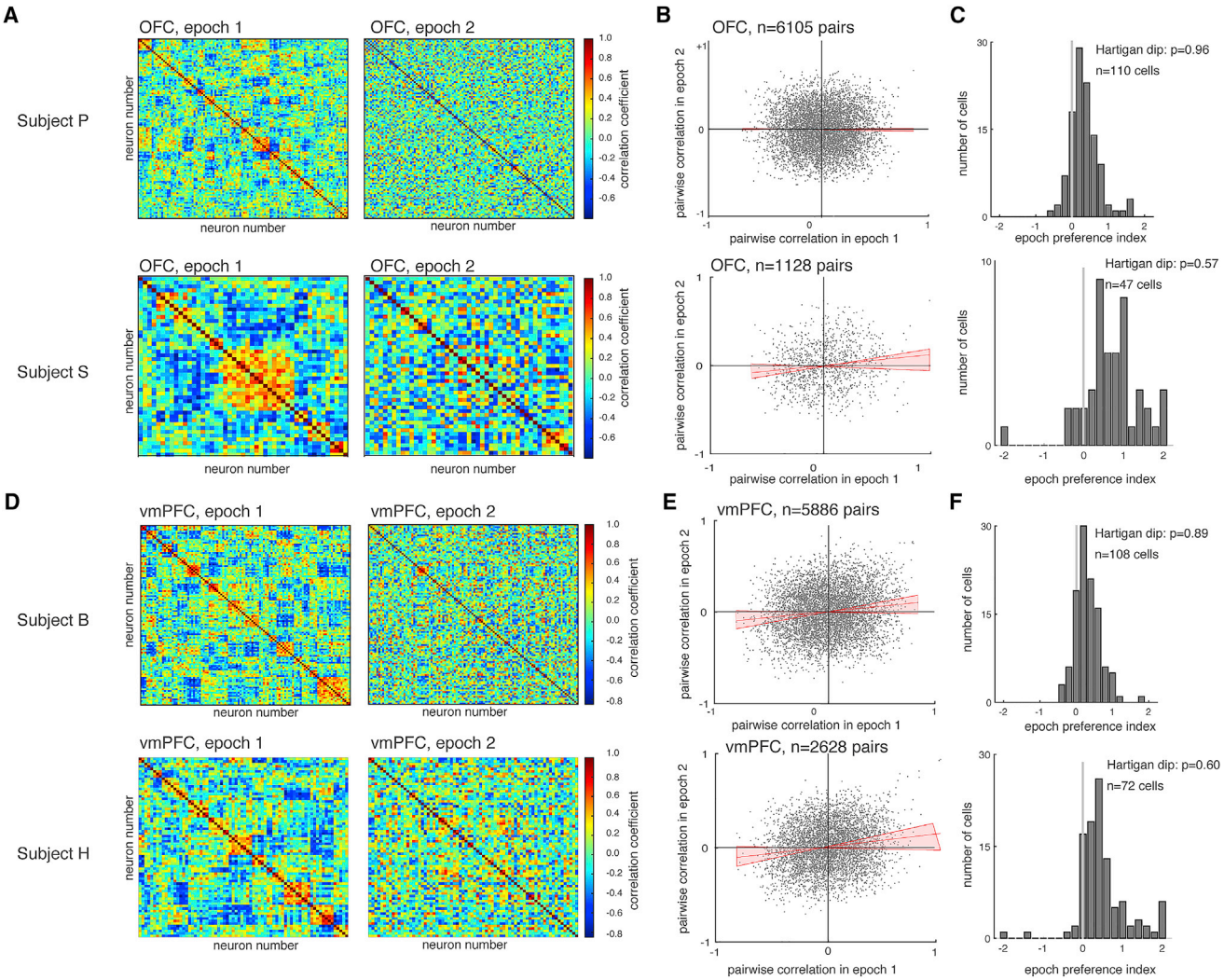

Figure 2. Covariance Structures Differ between Epoch 1 and Epoch 2 in Both OFC and vmPFC Populations

(A) Covariance matrices for epochs 1 (left) and 2 (right) in OFC. The entries in the x and y axes correspond to individual neurons; neurons are sorted according to an agglomerative hierarchical cluster tree algorithm on epoch 1, but not epoch 2 response patterns (see STAR Methods). Z axis indicates the strength of correlation between the overall average activities of those two neurons. Lack of obvious structure in epoch 2 matrix reflects strong functional reorganization between epochs 1 and 2.

(B) Scatterplot illustrating the relationship between correlation strengths for each pair of neurons in epochs 1 and 2. The very low correlations indicate that the relationship between neurons changes dramatically with epoch. Error bar is 95% confidence interval.

(C) Bar graph showing the distribution of the epoch preference index, a measure of the relative strength of firing from epoch 1 to 2 (see STAR Methods). The populations show no significant bimodality.

(D) Same results as in (A) but for vmPFC instead of OFC.

(E) Same result as in (B) but for vmPFC instead of OFC.

(F) Same result as in (C) but for vmPFC instead of OFC.

0.0134 ± 0.002 for subject H; OFC: R^2 = 0.009 ± 0.0001 for subject P and R^2 = 0.02 ± 0.0001 for subject S. These measures are all much less than 1.0 (i.e., from collinearity; $p < 0.001$ in all cases). Critically, these plots demonstrate a lack of correlation between these variables, as indicated both by the zero slope of the correlation lines and by the overlap of the error regions with the horizontal axis in all cases. This result suggests that the population in both regions substantially reconfigures their pairwise relationships as the subject shifts from the first to the second epoch of the task.

A Single Pool of Neurons for the Two Epochs

One factor that could explain the uncorrelated covariance structures is that a separate pool of neurons is activated in each epoch, perhaps corresponding to anatomical separation of function. We have previously explored the question of functionally

separate pools within economic regions using three different approaches (Azab and Hayden, 2017; Blanchard et al., 2015, 2018; Strait et al., 2014). In all cases, our data supported the idea that neurons selective for the variables relevant to evaluation and selection come from a single pool rather than two different pools (Hayden and Moreno-Bote, 2018).

The most straightforward test is as follows: if the same pools of neurons are active during both epochs, then the correlation between unsigned (absolute value) regression weights from epoch 1 neural activity against offer 1 and epoch 2 neural activity against offer 2 will be positive, whereas if there are separate populations of neurons, it will be negative. We use a method developed in Blanchard et al. (2015). The method uses the correlation of unsigned tuning strengths (regression of *Z* scored firing rates in a 400-ms offer period against offer value). We found a positive correlation for both OFC ($r = 0.2941$; $p < 0.001$) and vmPFC ($r = 0.3759$; $p < 0.001$). This positive correlation is consistent with the idea that, within each region, neurons involved in coding the two variables come from the same population of cells and, more formally, indicate that their constituent populations overlap more than expected by chance.

Elsayed and colleagues devised a novel method that can robustly delineate functional subpopulations based on response variability. Their method does not take into account tuning, meaning it rests on fewer assumptions than our approaches mentioned above and may therefore be more robust (Elsayed et al., 2016). The logic of this analysis is that, if a neuron shows preferential selectivity for one epoch, then the range of firing rates across trials will differ more during that epoch. The variance in the firing within an epoch then gives a measure of task selectivity that is entirely agnostic about what variables may be driving the firing. They used this method to demonstrate that preparatory and executive-movement-related activity in both premotor and motor cortex come from a single pool.

Using this method, we computed the difference between the range of firing rates in both epochs (epoch preference index; positive: preference for epoch 1; negative: preference for epoch 2; see STAR Methods). We then tabulated the population epoch-preference measures for the population. If the resulting distribution (across neurons) is bimodal, we can infer that discrete offer 1 and offer 2 populations exist. In our dataset, however, we observe distributions that are clearly unimodal, precisely the result we would observe if the neurons came from a single pool (Figures 2B and 2E). Measures of bimodality for these distributions strongly support unimodality (Figures 2C and 2F; Hartigan's dip test for vmPFC: $p = 0.9$ for subject B and $p = 0.63$ for subject H; for OFC: $p = 0.88$ for subject P and $p = 0.57$ for subject S).

The overall value of epoch preference index is positive (mean epoch preference for vmPFC subject B: 0.3033 and subject H: 0.4956; mean for OFC subject P: 0.3321 and subject S: 0.7229; $p < 0.05$ by rank-sum test for all subjects). This suggests that the neural population changes its activity more in epoch 1 with respect to the baseline firing rate of the neurons. It might suggest that the neural activity in epoch 2 might travel through more confined (or refined) neural subspace compared to the one that characterized epoch 1.

Core Reward Regions Use Nearly Orthogonal Subspaces for the Two Epochs

We tested the relationship between subspaces for the two epochs using a method developed for motor regions (Elsayed et al., 2016). We began with a standard dimensionality reduction technique, principal-component analysis (PCA). If the subspaces occupied by OFC or vmPFC neurons during offer 1 and offer 2 are orthogonal, then offer 1 epoch principal components (PCs) will necessarily capture little offer 2 neural data variance and vice versa. If the subspaces are the same, as would be predicted by standard threshold models, then cross-epoch PCs will be essentially indistinguishable from within-epoch PCs.

We focused on the top ten PCs under the assumption that they will account for most of the variance. Indeed, we found that the top ten PCs explained more than 90% of the variance in each of epoch 1 and epoch 2 in our OFC sample and about 90% of the variance in our vmPFC sample (Figures 3A, 3B, 3D, and 3E). However, the top ten PCs in epoch 1 captured very little epoch 2 neural data variance in OFC (OFC: 10.83% ± 0.083% for subject P; 35.85% ± 0.069% for subject S). Errors here are computed as the SD of leave-one-out cross-validation (see STAR Methods). Likewise, the top ten epoch 2 PCs captured very little epoch 1 neural data variance (OFC: 11.10% ± 0.024% for subject P; 38.69% ± 0.120% for subject S). We observed similar results in vmPFC (25.12% ± 0.103% and 27.56% ± 0.175% for subject B; 25.96% ± 0.051% and 24.48% ± 0.063% for subject H). This finding reveals that both regions use largely orthogonal coding schemes to encode information in the two epochs.

We next sought to determine whether this measured change reflects a true change in subspace or whether it is an artifactual consequence of the noise properties of our data. To do this, we performed the following cross-validation procedure to estimate statistical significance. We first computed a covariance matrix *within* epoch (specifically, within epoch 1) in a randomly subsampled set of trials (50% of all trials in each bin). We then computed an analogous covariance matrix *across* epochs on matched subsampled (i.e., 50% randomly decimated) trials. We then correlated these covariance matrices (using Pearson correlation) and repeated the process (with new randomization) 1,000 times. We found that measured correlations were greater than pseudocorrelations (mean R^2 from bootstrap OFC; subject P: 0.001 ± 0.004; S = 0.003 ± 0.006; vmPFC, subject B = 0.001 ± 0.003; subject H: 0.0363 ± 0.01). These ranges refer to 95% confidence intervals and thus can be considered significant at $p < 0.025$ (given the assumption of a one-sided t test).

We quantified the degree of change across the two epochs by calculating an "alignment index": the offer 1 epoch data variance captured by the top ten epoch 2 PCs, normalized by the epoch 1 data variance captured by the top ten epoch 1 PCs (see STAR Methods; Figures 3C and 3F). If the PCs for each epoch do not overlap, the index will be 0; if they overlap completely, the alignment index will be 1. The alignment index in vmPFC epoch 1 is 0.2641 and epoch 2 is 0.3124. Both of these numbers are significantly lower than the alignment index derived from randomly generated neural sample ($p < 0.003$ and $p = 0.038$, respectively; STAR Methods). For OFC, the alignment indices were 0.1473 and 0.1123 in the first and second epochs

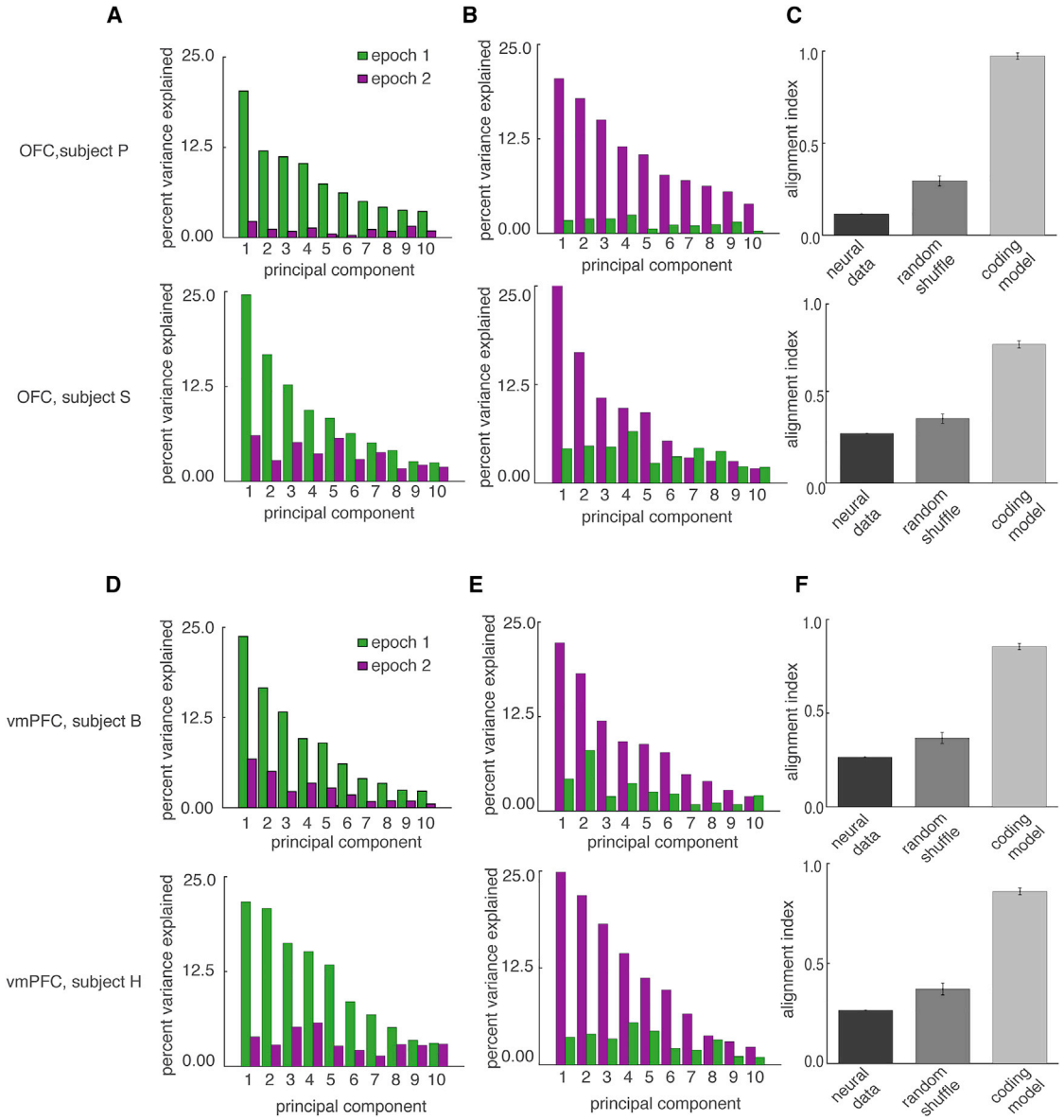

Figure 3. Demonstration that Neural Subspaces for Epochs 1 and 2 Are More Orthogonal Than Would Be Expected by Chance

(A) Plot of percent variance explained by each of the top ten principal components (PCs) for epoch 1 projected data projected onto epoch 1 subspace in OFC (green bars). Corresponding results from epoch 2 projected onto epoch 1 subspace are shown with purple bars. The low height of the purple bars relative to the green bars illustrates the poor match between subspaces for epochs 1 and 2.

(B) Neural activity from epoch 1 (green) and epoch 2 (purple) onto epoch 2 subspace.Confidence intervals for random and coding model are obtained by 10,000 resampling via bootstrapping ($p < 0.001$; sign-rank test).

(C) Bar graph showing that alignment of subspaces (as estimated by alignment index; see STAR Methods) across epochs (left bar) is significantly lower than the alignment associated with random data (middle bar) and the alignment obtained from a virtual population constructed by a coding model (right bar; see Results). Data are significantly lower than those obtained assuming a null hypothesis.

(D) Same analysis as in (A) but for vmPFC instead of OFC.

(E) Same analysis as in (B) but for vmPFC instead of OFC.

(F) Same analysis as in (C) but for vmPFC instead of OFC.

Confidence intervals for random and coding model are obtained by 10,000 resampling via bootstrapping ($p < 0.001$; sign-rank test).

(both $p < 0.001$). For both subjects, the index was significantly lower than randomly generated data (see STAR Methods), indicating that epoch 1 and epoch 2 responses occupy two near-orthogonal subspaces.

The data bars indicate a significantly lower alignment index than both the random and coding models. The confidence interval for random and coding model is obtained by 10,000 resampling via bootstrapping method ($p < 0.001$; sign-rank test).

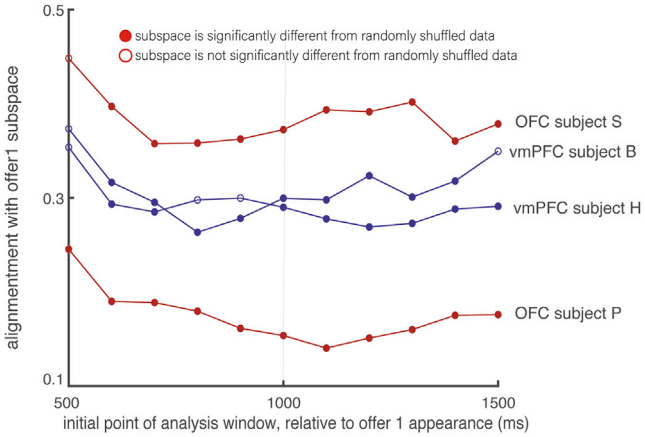

Figure 4. Change of Alignment Index over Time

Plot of the alignment between offer 1 subspace and subspace associated with each specific window in a sliding window analysis (window length: 400 ms; stride length, 100 ms). Values along the x axis refer to the starting point of the analysis window (the stopping point is therefore +400 ms). The y axis indicates alignment index (calculated identically to Figure 3). Filled circles indicate value that is significantly different from the 95% confidence interval range from 100 random shuffle data. Red lines: OFC; blue lines: vmPFC. If the reorganization is abrupt, then the change of alignment index should be step like. Instead, we observe a gradually changing curve.

To go into a bit more detail, essentially what coding model does is to select out number of trials from real data and calculate the regression between their firing and expected value. This guarantees that the value fed into Poisson spike generator is based on real neuronal data. Then "expected_value × beta" is fed into Poisson spike generator and spike was generated. Then the alignment index between epoch 1 pseudodata and epoch 2 pseudodata is calculated. This is then repeated 10,000 times.

We then estimated the principle angle between these subspaces using a previously published method (Knyazev and Argentati, 2002). In our method, we try to find all minimum principal angles between two subspaces spanned by the columns of matrices and calculated minimum value arc cosine value of the principal angle of each vector, a quantity that is sometimes called the canonical correlations. We find the neural subspace of epoch 1 and epoch 2 resulted in negligible value (near zero), in which smaller value means closer to orthogonal (mean of principal angle for OFC subject P: 1.32×10^{-15}, subject S: 1.31×10^{-15}; mean of principal angle for vmPFC subject B: 1.27×10^{-15}, subject H: 1.35×10^{-15}).

Note that these results indicate an adjustment toward orthogonality but do not imply a complete orthogonalization. That is, they indicate a strong change in subspace occupied, but not that this change is complete. Indeed, these results suggest that subspace reorganization in OFC and vmPFC are not complete, which differentiates these regions from, for example, primary motor cortex (Elsayed et al., 2016).

Repeating Analysis to Subset of Neurons

We then repeated this analysis but only on the subset of neurons that showed selectivity for the expected value of the offer 1 (as defined by a $p < 0.05$ by general linear regression). The alignment index was still different than the randomly shuffled data (OFC subject P: 0.2578 [95% confidence interval: 0.3133–0.3241]; subject S: 0.5523 [95% confidence interval: 0.5569–0.5715]; vmPFC subject B: 0.3333 [95% confidence interval: 0.3504–0.3615]; subject H: 0.3177 [95% confidence interval: 0.3479–0.3604]). The result was qualitatively similar to the one obtained from the full dataset. That is, we find orthogonality between the epoch 1 and epoch 2.

Comparison with Accumulator Model

We next sought to gain more insight into the relevance of these results in terms of standard ideas in the field. We reasoned that, among conventional approaches to understanding economic choice, the accumulation model is the most common one. We therefore implemented an evidence accumulation model with 100 pseudoneurons (see STAR Methods). Our implementation is designed to be as general as possible and is based, most specifically, on that of Philiastides et al. (2006). The three biggest assumptions made by our evidence accumulation model are that (1) there are no separate population of neurons tuned for offer 1 and offer 2 (this idea is justified by previous studies by us and others; e.g., Krajbich et al., 2010; Lim et al., 2011; Rich and Wallis, 2016; Strait et al., 2014, 2015; Xie et al., 2018), (2) the tuning of each neuron is preserved as the subject moves from attending to the first to the second offer (ibid.), and (3) the SD for accumulating evidence is constant over time. Assumptions (2) and (3) are also made in Philiastides et al. (2006). Other parameters that cannot, even in principle, affect subspace reorganization are excluded for simplicity; for example, we do not include the initial starting point of diffusion (Philiastides et al., 2006). We then calculated alignment index for these pseudodata. We find that the alignment index is not significantly different from the alignment index for randomly shuffled simulated data: index = 0.8229; median of random alignment index from 1,000 simulations) and significantly different from the randomly shuffled data (95% confidence interval of random shuffle is 0.4888–0.4925). In other words, the model's outcome is significantly different than random (thus, $p < 0.05$).

Dynamics of Subspace Reorganization

We next asked about the dynamics of this subspace reorganization (Figure 4). We therefore repeated the process by a sliding window approach (window size: 400 ms; stride length: 100 ms). This analysis demonstrates a gradualness to the transition of neural subspace. Specifically, the shape of the curve, in which the y axis was alignment index, was unlike the step function. Instead, the alignment index appears to decrease continuously until a relatively late time point (note that the smaller alignment index means more orthogonal).

In considering dynamics, we also considered the period after the second offer epoch, the "both offers" period. We used the epoch from 3.125 s to 3.525 s, where both offers were simultaneously presented (we call this epoch 3). We found that neural subspace of epoch 3 is reorganized compared to both epoch 1 and 2. This is shown by significant alignment index values (epoch 1 versus epoch 3 in OFC subject P: 0.1515 [95% confidence interval: 0.2892–0.3515], subject S: 0.3669 [95% confidence interval: 0.4036–0.4186]; epoch 1 versus epoch 3 in vmPFC subject

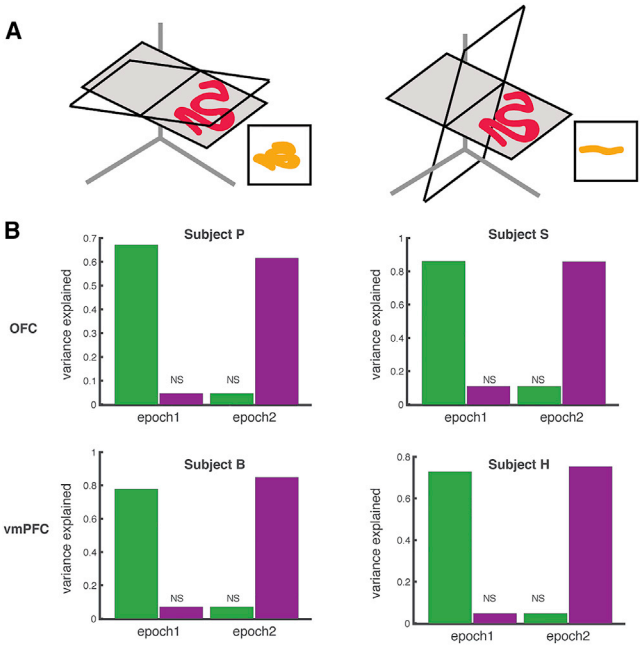

Figure 5. Construction of Fully Orthogonal Subspace via Objective Function Maximizing Orthogonality within Epoch and across the Epoch

(A) Schematic display of possible relationship between the subspaces. If the spaces are nearly collinear (left), then a projection of responses from one subspace to the other will be nearly veridical. But if they are fully orthogonal (right), the activity span over one subspace will not show significant variance in the other subspace.

(B) For all subjects and both areas, cross-epoch projection reduces variance explained. Plot shows percentage of variance explained by the epoch 1 (green) and epoch 2 (purple) subspaces with constraints imposed by the objective function. The left pair of bars corresponds to variance captured during the epoch 1. The right pair of bars corresponds to variance captured during the epoch 2 (NS, not significant). The significance was tested by 1,000 time bootstrapping.

B: 0.2922 [95% confidence interval: 0.3458–0.3577]; subject H: 0.2897 [95% confidence interval: 0.3650–0.3788]; epoch 2 versus epoch 3 in OFC subject P: 0.1512 [95% confidence interval: 0.2885–0.3003]; subject S: 0.4123 [95% confidence interval: 0.4180–0.4323]; epoch 2 versus epoch 3 in vmPFC subject B: 0.2996 [95% confidence interval: 0.3498–0.3618]; subject H: 0.3292 [95% confidence interval: 0.3699–0.3818]).

These confidence intervals do not span or even approach the value of 1.0; this fact means they can be said to be at least partially orthogonalized, at a $p < 0.025$, given the assumption of one-sided test. Our results have the same interpretation regardless of whether the decision is made covertly before it is expressed (as is proposed in, for example, Azab and Hayden, 2017). If neurons move from encoding offered values to encoding chosen values, their firing rates will change and their tuning will change, but their subspace will not. The same logic applies if they switch to encoding other task variables, such as value sum, value difference, or unchosen value. These changes would alter the referent of the neurons' firing rates but would not change the way that the firing of pairs of neurons relate to each other.

Controlling for Possible Confounds Introduced by Cross-Epoch Heteroscedasticity

The weak predictive relationship between the epoch 1 PCs and epoch 2 PCs supports our core hypothesis of a change in subspace occupancy that varies with change in function. One possible confound comes from the fact that this method is potentially sensitive to the relative amount of activity variance of the two neural population responses in each epoch. Another possible confound comes from the fact that our previous method may partially inflate measures of orthogonality (Elsayed et al., 2016). Because epoch-1- and epoch-2-related computations take place in nearly orthogonal subspaces, it should be possible to isolate those computations by projecting the full population responses onto the two subspaces (note that this separation would not be generally achievable if they involve overlapping subspaces, which would make it impossible to separate epoch 1 and epoch 2 activity via linear projections).

By using a method that specifies subspaces with an objective function that maximizes orthogonality within and across epochs, we can construct subspaces that are fully orthogonal to each other. That is, our approach solves the "generalized eigenvalue problem" (Boumal et al., 2014; Cunningham and Ghahramani, 2014). Using this method, we found that each epoch can occupy fully non-overlapping orthogonal spaces (Figure 5). Specifically, we identified four epoch 1 dimensions in OFC (which captured 67% and 83% of the epoch 1 variance for monkey P and S, respectively) and four epoch 1 dimensions in vmPFC (which captured 75% and 74% of the epoch 1 variance for monkey B and H, respectively). Similarly, we identified five epoch 2 dimensions for OFC (which captured 60% and 83% of the epoch 2 variance for monkey P and S, respectively) and five epoch 2 dimensions for vmPFC (which captured 83% and 75% of the epoch 2 variance for monkey B and H, respectively). Not surprisingly, most neurons contributed to both the epoch 1 and epoch 2 subspaces. This result confirms that the subspace associated with each epoch is distinct. Note that, to estimate significance for these analyses, we used a multiple bootstrap procedure (n = 500 bootstraps). Specifically, we selected a random subset of trials, then did a nonlinear subspace formation for epoch 1 and epoch 2, and then reprojected them. Then, we repeated this step 500 times. If the distribution of variance explained was not different from chance level, then we designated the result as non-significant.

Relationship between the Subspaces: Orthogonal but Functionally Linked

The reorganization of subspaces raises the question of how the coding scheme itself changes across epochs. Does it also show a similar rotation? More formally, does the change from epoch 1 to epoch 2 alter the order (or mapping) between offer value and population firing rates? This question is important because standard null-space approaches imagine reordering (Kaufman et al., 2014), but our past data in these regions in this and similar tasks suggest a preservation of coding (Azab and Hayden, 2017, 2018; Blanchard et al., 2015; Strait et al., 2014).

We answered this question using linear decoder. Specifically, we wanted to ask how well the pattern of epoch 1 activity could be predicted from the pattern of epoch 2 activity in fully

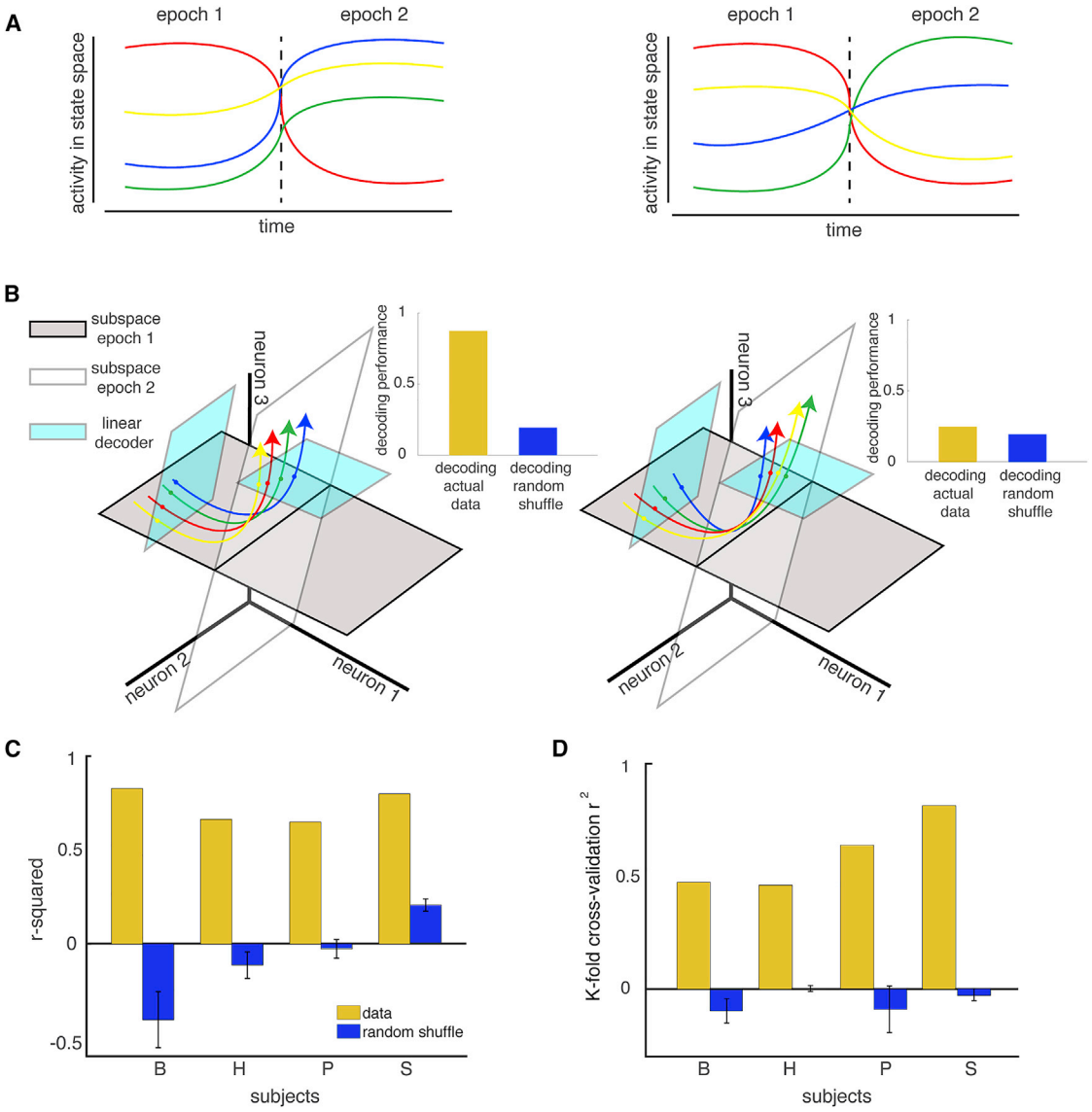

Figure 6. The Orderly Transition of Neural Activity between the Subspaces

(A) Activity values at state space as a function of time. The color of each trace indicates the condition, which in our task is offer expected value. The first/second half of each trace (before/after the dashed line) corresponds to the response to that value in the first/second epoch. The key idea is that, following the transition to epoch 2, there is still a lawful relationship, even though the order is flipped.

(B) Cartoon of this idea in 3-space. Each dimension refers to activity of a neuron (and this idea extends to higher dimensions). When moving from epoch 1 to epoch 2, activity in state space evolves from subspace of epoch 1 to subspace of epoch 2. We can train a linear decoder (blue rectangle) in epoch 1 subspace and then predict the order at subspace of epoch 2. Subset panel shows expected result.

(C) The actual result of linear decoder performance. Quality of fit (r^2) of the regression between the responses in the epoch 2 subspace (in the middle of epoch 2) and the responses in the epoch 1 subspace (at the end of the epoch 1). Error bars denote the 95% confidence interval of the 1,000 times bootstrapped data.

(D) Leave-one-out cross-validation (LOOCV) analysis of the same data as (C).

orthogonalized subspaces. We used the neural state in one time window in epoch 1 (400 ms after offer 1 onset for both brain areas) to predict, using a simple linear decoder (see STAR Methods), the neural state in epoch 2 (time 250 ms after offer 2 presentation for vmPFC and for OFC). The shuffled data were treated as the baseline; shuffling occurred at the trial level (we chose these epochs *a priori* specifically to avoid overlap with other cognitively relevant processes, like the start of the trial and the choice saccade). Despite the simplicity of the decoder and the fact that epoch 1 and epoch 2 responses occupy orthogonal subspaces, the quality of the prediction was high (vmPFC: R^2 = 0.8276 for subject B, R^2 = 0.6630 for subject H; OFC: R^2 = 0.6491 for subject P, R^2 = 0.7987 for subject S; Figure 6C).

To test whether the predictability between the activity pattern in each subspace can be generalized, we performed k-fold cross-validation (where k was 30, which was the minimum

number of trials in certain session) and calculated the R^2 value between activity in epoch 1 and epoch 2 (Figure 6D). For the process, we left out some trials from each condition and designated as test data. The original data resulted in larger value than zero (R^2 for vmPFC subject B: 0.4737 and subject H: 0.4608; R^2 for OFC subject P: 0.6423 and subject S: 0.8142). When we shuffle the data, all the R^2 became smaller than zero and its confidence interval overlapped with zero. This similarity indicates the patterns of neural activity in epoch 1 are conserved following the transition to epoch 2, even as the subspace rotates. The robustness of this finding is demonstrated by the fact that this relationship is observed in test conditions that were not used to fit the decoder.

DISCUSSION

Here, we compared the firing rate subspaces occupied by ensembles of neurons in two core reward regions, OFC and vmPFC, during two phases of a choice task. We find that the covariance matrix (the set of firing rate relationships between all pairs of neurons) changes to become more orthogonal as the subject moves from the first (ostensible evaluation) epoch to the second (ostensible selection) one. At the same time, the population of neurons involved does not change (that is, these regions used a single pool rather than two pools), nor does the ensemble tuning structure change. These results point to a possible solution to a critical, but often ignored, problem in neuroeconomics: the need to selectively gate value representations. During economic choice, value computations should inform and ultimately drive selection processes. But the brain faces a "gating problem": in cases where values are computed asynchronously, values computed earlier must be prevented from driving premature selection. This problem is well known in systems engineering, but it is equally relevant to economic choice. Subspace rotation accomplishes this by allowing neurons in both regions to strongly encode values in a manner that does not risk driving choice because those value encodings, at the ensemble level, are in a pattern orthogonal to one that leads to selection (cf. Hannah et al., 2018; Kaufman et al., 2014; Khanna et al., 2019; Stavisky et al., 2017).

Our results explain effective responding in contexts in which options are contemplated asynchronously rather than simultaneously. Although simultaneous encounter is common in the laboratory, there is a good deal of evidence that natural decision making evolved based on the principle of sequential encounter (Freidin et al., 2009; Kacelnik et al., 2011; Stephens and Krebs, 1986). As such, our decision-making hardware is likely constructed to function in sequential choice contexts (Hayden, 2018; Stephens and Anderson, 2001). Moreover, there is some evidence that, in cases that provide ostensibly simultaneous offers, we contemplate them serially regardless, meaning that the gating problem may be a more general one than it initially appears (Krajbich and Rangel, 2011; Lim et al., 2011; Rich and Wallis, 2016; Hayden, 2018). The robustness of serial choice may be a consequence of the limits of the focal spotlight of selective attention, which is likely to be required to implement the complex calculations associated with assigning values to offers (Hayden and Moreno-Bote, 2018; Krajbich and Rangel, 2011).

In any case, the reorganization we observe occurs rapidly. This speed suggests it does not reflect changes in wiring or in receptor patterns but rather reflects much more rapid changes in neural computational properties. These results, if correct, resemble others showing that rapid connectivity changes underlie key brain state changes, even outside the motor system (Ebitz et al., 2018; Mante et al., 2013; Stokes et al., 2013). Our findings also suggest that neural space at each epoch may not be random but may reorganize in a principled way. Specifically, the neural subspace associated with epoch 2 appears to be constrained by (or, equivalently, a refined version of) the neural subspace occupied at epoch 1. This, indeed, can be a potential neural mechanism for the "relative valuation hypothesis" (Hayden and Moreno-Bote, 2018). In the theory explaining sequential decision making, the option appearing second would be computed in a way that depends on the value of the first option.

The design of our task does not require subjects to transition from evaluation to selection when the second offer appears. Nonetheless, there are a few reasons to think they do so. First, neuronal responses during the second epoch are selective for the values of both individual offers (and at roughly the same intensity), indicating that the second is stored in working memory at this time and thus is available for comparison (Azab and Hayden, 2017, 2018; Strait et al., 2014). Second, in a control task in which we did not show the options again, subjects were able to choose well, meaning they must have maintained the value of both offers in working memory (see Results). Third, neurons' firing rates were sensitive to the value difference between the options, indicating that their neurons, at least, were engaging in value comparison (Strait et al., 2014; Results). Indeed, variability in firing rate predicted variability in choice, suggesting an association between these relative value signals and expressed preferences (Strait et al., 2014). Finally, and most importantly, responses of neurons in vmPFC, as well as another region implicated in choice, the dorsal anterior cingulate cortex (dACC), show qualitative ensemble response changes that reflected the completed choice early in the second epoch (Azab and Hayden, 2017). Specifically, the association between ensemble tuning for offer value for chosen and rejected offers changes from being collinear to being orthogonal, indicating that choice is complete during that offer epoch. Together, these four findings support the idea that the second offer epoch hosts the selection stage of choice.

The neuroeconomic gating problem is analogous to other problems in the brain. In particular, the motor system shows clear motor-related activity prior to the initiation of movement. The brain must gate this preparatory activity to prevent it from driving behavior prematurely (Elsayed et al., 2016; Kaufman et al., 2014). Preparatory movements in both motor and premotor cortex occupy an output-null dimension, and the dimension rotates within the region at the time of transition to execution (Kaufman et al., 2014). A similar subspace rearrangement occurs in the oculomotor system (frontal eye field; Khanna et al., 2019). Finally, in primate motor cortex and premotor cortices, precocious movement is gated by subspace orthogonalization (Elsayed et al., 2016). Our results, which show preserved ensemble value tuning across epochs, qualitatively resemble those of Elsayed more than the others, but share with all of

them the idea that it is the use of an output-null state rather than rise to threshold that serves the gating function.

In light of these findings in motor regions, our results suggest that the brain makes use of common computational motifs to solve similar problems in distinct regions. These results do not imply, however, that areas 13 and 14 are functionally identical to each other or to motor regions. Instead, we suspect that the relationship between them is that between two different points along a larger continuum proceeding from an input (sensory) to output (motor) end (Strait et al., 2016; Yoo et al., 2018, 2019; Yoo and Hayden, 2018). That is, they likely have quantitative, but not qualitative, differences, at least for the core choice-related functions we study here. Indeed, they likely *do* have qualitative differences with regards to other functions, and those should, in principle, be predictable from their connectivity. For example, Bradfield and Hart (2019) have proposed that these regions both participate in encoding a cognitive map of state space but have an emphasis on initial and anticipated future positions, respectively. For other examples, see compelling cases made by Bouret and Richmond (2015), Monosov and Hikosaka (2012), and Noonan et al. (2010). A critical question for future study is whether OFC should be placed earlier in a processing hierarchy than vmPFC, or vice versa, or whether they are better thought of as separate inputs to the larger choice system, respectively supporting sensory and visceral influences on choice (Ongür and Price, 2000).

Recent years have seen a revolution in our understanding of the motor cortex (Cisek, 2012; Fetz, 1992; Shenoy et al., 2013). Many motor physiologists have moved away from the encoding model in favor of a dynamical systems perspective (Cunningham and Yu, 2014; Gallego et al., 2017). In other words, these motor physiologists have abandoned a representational view of motor control and replaced it with a functional view (Gallego et al., 2017; Golub et al., 2018; Hennig et al., 2018; Semedo et al., 2019; Pandarinath et al., 2018; Sadtler et al., 2014; Sussillo et al., 2015). We believe that it is time for a similar antirepresentationalist revolution to occur within neuroeconomics (Hunt and Hayden, 2017; Yoo and Hayden, 2018). From this perspective, we may want to consider the so-called core reward regions as intermediate layers of a larger brain network whose computations serve to produce actions (Figure 6; Cisek, 2012; Cisek and Kalaska, 2010; Eisenreich et al., 2017; Pearson et al., 2014; Pezzulo and Cisek, 2016; Yoo and Hayden, 2018). That is, we suspect that neuroeconomics may best be able to advance by seeing the economic regions as regulatory structures that govern the premotor regions in the same way the premotor regions regulate the motor regions (Cisek, 2012; Heilbronner and Hayden, 2016a).

STAR★METHODS

Detailed methods are provided in the online version of this paper and include the following:

- KEY RESOURCES TABLE
- LEAD CONTACT AND MATERIALS AVAILABILTY
- EXPERIMENTAL MODEL AND SUBJECT DETAILS
- METHOD DETAILS
  - Electrophysiological techniques, eye tracking, and reward delivery
  - Behavioral task
  - Data preprocessing
  - Epoch preference index
  - Pairwise cross-condition correlation
  - Significance test for epoch comparison
  - The evidence accumulation model
  - Subspace overlap analysis
  - Invariant encoding model
  - Advanced method for demonstrating fully orthogonal subspace
  - Analytical technique demonstrating linked relationship between the epoch
- DATA AND CODE AVAILABILITY

ACKNOWLEDGMENTS

We thank Caleb Strait, Maya Wang, Tyler Cash-Padgett, and Marc Mancarella for help in data collection. We appreciate Cindy Tu for discussion at initial stage. We thank Alex Herman for useful help with writing. This project was supported by a grant from the NIH (NIDA 038615).

AUTHOR CONTRIBUTIONS

B.Y.H. conceptualized and designed the experiment. S.B.M.Y. analyzed the data. S.B.M.Y. and B.Y.H. wrote the manuscript.

DECLARATION OF INTERESTS

The authors declare no competing interests.

Received: May 31, 2019
Revised: October 13, 2019
Accepted: November 8, 2019
Published: December 10, 2019

REFERENCES

Azab, H., and Hayden, B.Y. (2017). Correlates of decisional dynamics in the dorsal anterior cingulate cortex. PLoS Biol. *15*, e2003091.

Azab, H., and Hayden, B.Y. (2018). Correlates of economic decisions in the dorsal and subgenual anterior cingulate cortices. Eur. J. Neurosci. *47*, 979–993.

Bartra, O., McGuire, J.T., and Kable, J.W. (2013). The valuation system: a coordinate-based meta-analysis of BOLD fMRI experiments examining neural correlates of subjective value. Neuroimage *76*, 412–427.

Blanchard, T.C., and Hayden, B.Y. (2014). Neurons in dorsal anterior cingulate cortex signal postdecisional variables in a foraging task. J. Neurosci. *34*, 646–655.

Blanchard, T.C., Hayden, B.Y., and Bromberg-Martin, E.S. (2015). Orbitofrontal cortex uses distinct codes for different choice attributes in decisions motivated by curiosity. Neuron *85*, 602–614.

Blanchard, T.C., Piantadosi, S., and Hayden, B.Y. (2018). Robust mixture modeling reveals category-free selectivity in reward region neuronal ensembles. J. Neurophysiol. *119*, 1305–1318.

Boumal, N., Mishra, B., Absil, P.-A., and Sepulchre, R. (2014). Manopt, a Matlab toolbox for optimization on manifolds. J. Mach. Learn. Res. *15*, 1455–1459.

Bouret, S., and Richmond, B.J. (2015). Sensitivity of locus ceruleus neurons to reward value for goal-directed actions. J. Neurosci. *35*, 4005–4014.

Bradfield, L.A., and Hart, G. (2019). Medial and lateral orbitofrontal cortices represent unique components of cognitive maps of task space. PsyArXiv. https://doi.org/10.31234/osf.io/tk5gn.

Calhoun, A.J., and Hayden, B.Y. (2015). The foraging brain. Curr. Opin. Behav. Sci. *5*, 24–31.

Chau, B.K.H., Kolling, N., Hunt, L.T., Walton, M.E., and Rushworth, M.F.S. (2014). A neural mechanism underlying failure of optimal choice with multiple alternatives. Nat. Neurosci. *17*, 463–470.

Chen, X., and Stuphorn, V. (2015). Sequential selection of economic good and action in medial frontal cortex of macaques during value-based decisions. eLife *4*, 1–24.

Churchland, M.M., Cunningham, J.P., Kaufman, M.T., Ryu, S.I., and Shenoy, K.V. (2010). Cortical preparatory activity: representation of movement or first cog in a dynamical machine? Neuron *68*, 387–400.

Cisek, P. (2012). Making decisions through a distributed consensus. Curr. Opin. Neurobiol. *22*, 927–936.

Cisek, P., and Kalaska, J.F. (2010). Neural mechanisms for interacting with a world full of action choices. Annu. Rev. Neurosci. *33*, 269–298.

Cooper, A.B., Pettorelli, N., and Durant, S.M. (2007). Large carnivore menus: factors affecting hunting decisions by cheetahs in the Serengeti. Anim. Behav. *73*, 651–659.

Crammond, D.J., and Kalaska, J.F. (2000). Prior information in motor and premotor cortex: activity during the delay period and effect on pre-movement activity. J. Neurophysiol. *84*, 986–1005.

Cunningham, J.P., and Ghahramani, Z. (2014). Linear dimensionality reduction: survey, insights, and generalizations. J. Mach. Learn. Res. *16*, 2859–2900.

Cunningham, J.P., and Yu, B.M. (2014). Dimensionality reduction for large-scale neural recordings. Nat. Neurosci. *17*, 1500–1509.

Ebitz, R.B., Albarran, E., and Moore, T. (2018). Exploration disrupts choice-predictive signals and alters dynamics in prefrontal cortex. Neuron *97*, 450–461.e9.

Eisenreich, B.R., Akaishi, R., and Hayden, B.Y. (2017). Control without controllers: toward a distributed neuroscience of executive control. J. Cogn. Neurosci. *29*, 1684–1698.

Elsayed, G.F., Lara, A.H., Kaufman, M.T., Churchland, M.M., and Cunningham, J.P. (2016). Reorganization between preparatory and movement population responses in motor cortex. Nat. Commun. *7*, 13239.

Farashahi, S., Azab, H., Hayden, B., and Soltani, A. (2018). On the flexibility of basic risk attitudes in monkeys. J. Neurosci. *38*, 4383–4398.

Fetz, E.E. (1992). Are movement parameters recognizably coded in the activity of single neuron? Behav. Brain Sci. *15*, 679–690.

Freidin, E., Cuello, M.I., and Kacelnik, A. (2009). Successive negative contrast in a bird: starlings' behaviour after unpredictable negative changes in food quality. Anim. Behav. *77*, 857–865.

Gallego, J.A., Perich, M.G., Miller, L.E., and Solla, S.A. (2017). Neural manifolds for the control of movement. Neuron *94*, 978–984.

Gold, J.I., and Shadlen, M.N. (2007). The neural basis of decision making. Annu. Rev. Neurosci. *30*, 535–574.

Golub, M.D., Sadtler, P.T., Oby, E.R., Quick, K.M., Ryu, S.I., Tyler-Kabara, E.C., Batista, A.P., Chase, S.M., and Yu, B.M. (2018). Learning by neural reassociation. Nat. Neurosci. *21*, 607–616.

Hannah, R., Cavanagh, S.E., Tremblay, S., Simeoni, S., and Rothwell, J.C. (2018). Selective suppression of local interneuron circuits in human motor cortex contributes to movement preparation. J. Neurosci. *38*, 1264–1276.

Hare, T.A., Camerer, C.F., and Rangel, A. (2009). Self-control in decision-making involves modulation of the vmPFC valuation system. Science *324*, 646–648.

Hayden, B.Y. (2018). Economic choice: the foraging perspective. Curr. Opin. Behav. Sci. *24*, 1–6.

Hayden, B.Y., and Gallant, J.L. (2013). Working memory and decision processes in visual area v4. Front. Neurosci. *7*, 18.

Hayden, B.Y., and Moreno-Bote, R. (2018). A neuronal theory of sequential economic choice. Brain Neurosci. Adv. *2*, 1–15.

Hayden, B.Y., Heilbronner, S.R., and Platt, M.L. (2010). Ambiguity aversion in rhesus macaques. Front. Neurosci. *4*, 1–7.

Hayden, B.Y., Pearson, J.M., and Platt, M.L. (2011). Neuronal basis of sequential foraging decisions in a patchy environment. Nat. Neurosci. *14*, 933–939.

Heilbronner, S.R., and Hayden, B.Y. (2016a). Dorsal anterior cingulate cortex: a bottom-up view. Annu. Rev. Neurosci. *39*, 149–170.

Heilbronner, S.R., and Hayden, B.Y. (2016b). The description-experience gap in risky choice in nonhuman primates. Psychon. Bull. Rev. *23*, 593–600.

Hennig, J.A., Golub, M.D., Lund, P.J., Sadtler, P.T., Oby, E.R., Quick, K.M., Ryu, S.I., Tyler-Kabara, E.C., Batista, A.P., Yu, B.M., and Chase, S.M. (2018). Constraints on neural redundancy. eLife *7*, 1–34.

Hunt, L.T., and Hayden, B.Y. (2017). A distributed, hierarchical and recurrent framework for reward-based choice. Nat. Rev. Neurosci. *18*, 172–182.

Hunt, L.T., Kolling, N., Soltani, A., Woolrich, M.W., Rushworth, M.F.S., and Behrens, T.E.J. (2012). Mechanisms underlying cortical activity during value-guided choice. Nat. Neurosci. *15*, 470–476, S1–S3.

Hunt, L.T., Dolan, R.J., and Behrens, T.E.J. (2014). Hierarchical competitions subserving multi-attribute choice. Nat. Neurosci. *17*, 1613–1622.

Semedo, J.D., Zandvakili, A., Machens, C.K., Yu, B.M., and Kohn, A. (2019). Cortical areas interact through a communication subspace. Neuron *102*, 249–259.e4.

Johnson, M.T.V., Coltz, J.D., and Ebner, T.J. (1999). Encoding of target direction and speed during visual instruction and arm tracking in dorsal premotor and primary motor cortical neurons. Eur. J. Neurosci. *11*, 4433–4445.

Kacelnik, A., Vasconcelos, M., Monteiro, T., and Aw, J. (2011). Darwin's "tug-of-war" vs. starlings' "horse-racing": How adaptations for sequential encounters drive simultaneous choice. Behav. Ecol. Sociobiol. *65*, 547–558.

Kaufman, M.T., Churchland, M.M., Ryu, S.I., and Shenoy, K.V. (2014). Cortical activity in the null space: permitting preparation without movement. Nat. Neurosci. *17*, 440–448.

Khanna, S.B., Snyder, A.C., and Smith, M.A. (2019). Distinct sources of variability affect eye movement preparation. J. Neurosci. *39*, 4511–4526.

Knyazev, A.V., and Argentati, M.E. (2002). Principal angles between subspaces in an A-based scalar product: algorithms and perturbation estimates. SIAM J. Sci. Comput. *23*, 2008–2040.

Krajbich, I., and Rangel, A. (2011). Multialternative drift-diffusion model predicts the relationship between visual fixations and choice in value-based decisions. Proc. Natl. Acad. Sci. USA *108*, 13852–13857.

Krajbich, I., Armel, C., and Rangel, A. (2010). Visual fixations and the computation and comparison of value in simple choice. Nat. Neurosci. *13*, 1292–1298.

Levy, D.J., and Glimcher, P.W. (2012). The root of all value: a neural common currency for choice. Curr. Opin. Neurobiol. *22*, 1027–1038.

Lim, S.-L., O'Doherty, J.P., and Rangel, A. (2011). The decision value computations in the vmPFC and striatum use a relative value code that is guided by visual attention. J. Neurosci. *31*, 13214–13223.

Mante, V., Sussillo, D., Shenoy, K.V., and Newsome, W.T. (2013). Context-dependent computation by recurrent dynamics in prefrontal cortex. Nature *503*, 78–84.

Mars, R.B., Verhagen, L., Gladwin, T.E., Neubert, F.X., Sallet, J., and Rushworth, M.F.S. (2016). Comparing brains by matching connectivity profiles. Neurosci. Biobehav. Rev. *60*, 90–97.

Meder, D., Kolling, N., Verhagen, L., Wittmann, M.K., Scholl, J., Madsen, K.H., Hulme, O.J., Behrens, T.E.J., and Rushworth, M.F.S. (2017). Simultaneous representation of a spectrum of dynamically changing value estimates during decision making. Nat. Commun. *8*, 1942.

Monosov, I.E., and Hikosaka, O. (2012). Regionally distinct processing of rewards and punishments by the primate ventromedial prefrontal cortex. J. Neurosci. *32*, 10318–10330.

Montague, P.R., and Berns, G.S. (2002). Neural economics and the biological substrates of valuation. Neuron *36*, 265–284.

Murray, E.A., O'Doherty, J.P., and Schoenbaum, G. (2007). What we know and do not know about the functions of the orbitofrontal cortex after 20 years of cross-species studies. J. Neurosci. *27*, 8166–8169.

Noonan, M.P., Walton, M.E., Behrens, T.E.J., Sallet, J., Buckley, M.J., and Rushworth, M.F.S. (2010). Separate value comparison and learning mechanisms in macaque medial and lateral orbitofrontal cortex. Proc. Natl. Acad. Sci. USA *107*, 20547–20552.

Noonan, M.P., Kolling, N., Walton, M.E., and Rushworth, M.F.S. (2012). Re-evaluating the role of the orbitofrontal cortex in reward and reinforcement. Eur. J. Neurosci. *35*, 997–1010.

Ongür, D., and Price, J.L. (2000). The organization of networks within the orbital and medial prefrontal cortex of rats, monkeys and humans. Cereb. Cortex *10*, 206–219.

Padoa-Schioppa, C. (2011). Neurobiology of economic choice: a good-based model. Annu. Rev. Neurosci. *34*, 333–359.

Padoa-Schioppa, C., and Cai, X. (2011). The orbitofrontal cortex and the computation of subjective value: consolidated concepts and new perspectives. Ann. N Y Acad. Sci. *1239*, 130–137.

Padoa-Schioppa, C., and Conen, K.E. (2017). Orbitofrontal cortex: a neural circuit for economic decisions. Neuron *96*, 736–754.

Padoa-Schioppa, C., Jandolo, L., and Visalberghi, E. (2006). Multi-stage mental process for economic choice in capuchins. Cognition *99*, B1–B13.

Pandarinath, C., O'Shea, D.J., Collins, J., Jozefowicz, R., Stavisky, S.D., Kao, J.C., Trautmann, E.M., Kaufman, M.T., Ryu, S.I., Hochberg, L.R., et al. (2018). Inferring single-trial neural population dynamics using sequential auto-encoders. Nat. Methods *15*, 805–815.

Papageorgiou, G.K., Sallet, J., Wittmann, M.K., Chau, B.K.H., Schüffelgen, U., Buckley, M.J., and Rushworth, M.F.S. (2017). Inverted activity patterns in ventromedial prefrontal cortex during value-guided decision-making in a less-is-more task. Nat. Commun. *8*, 1886.

Pearson, J.M., Watson, K.K., and Platt, M.L. (2014). Decision making: the neuroethological turn. Neuron *82*, 950–965.

Pezzulo, G., and Cisek, P. (2016). Navigating the affordance landscape: feedback control as a process model of behavior and cognition. Trends Cogn. Sci. *20*, 414–424.

Philiastides, M.G., Ratcliff, R., and Sajda, P. (2006). Neural representation of task difficulty and decision making during perceptual categorization: a timing diagram. J. Neurosci. *26*, 8965–8975.

Pirrone, A., Azab, H., Hayden, B.Y., Stafford, T., and Marshall, J.A.R. (2018). Evidence for the speed-value trade-off: human and monkey decision making is magnitude sensitive. Decision (Wash. D.C.) *5*, 129–142.

Polanía, R., Krajbich, I., Grueschow, M., and Ruff, C.C. (2014). Neural oscillations and synchronization differentially support evidence accumulation in perceptual and value-based decision making. Neuron *82*, 709–720.

Polanía, R., Woodford, M., and Ruff, C.C. (2019). Efficient coding of subjective value. Nat. Neurosci. *22*, 134–142.

Rangel, A., Camerer, C., and Montague, P.R. (2008). A framework for studying the neurobiology of value-based decision making. Nat. Rev. Neurosci. *9*, 545–556.

Rich, E.L., and Wallis, J.D. (2014). Medial-lateral organization of the orbitofrontal cortex. J. Cogn. Neurosci. *26*, 1347–1362.

Rich, E.L., and Wallis, J.D. (2016). Decoding subjective decisions from orbitofrontal cortex. Nat. Neurosci. *19*, 973–980.

Rushworth, M.F.S., Noonan, M.P., Boorman, E.D., Walton, M.E., and Behrens, T.E. (2011). Frontal cortex and reward-guided learning and decision-making. Neuron *70*, 1054–1069.

Rustichini, A., and Padoa-Schioppa, C. (2015). A neuro-computational model of economic decisions. J. Neurophysiol. *114*, 1382–1398.

Sadtler, P.T., Quick, K.M., Golub, M.D., Chase, S.M., Ryu, S.I., Tyler-Kabara, E.C., Yu, B.M., and Batista, A.P. (2014). Neural constraints on learning. Nature *512*, 423–426.

Schuck, N.W., Cai, M.B., Wilson, R.C., and Niv, Y. (2016). Human orbitofrontal cortex represents a cognitive map of state space. Neuron *91*, 1402–1412.

Shadlen, M.N.N., and Shohamy, D. (2016). Decision making and sequential sampling from memory. Neuron *90*, 927–939.

Shenoy, K.V., Sahani, M., and Churchland, M.M. (2013). Cortical control of arm movements: a dynamical systems perspective. Annu. Rev. Neurosci. *36*, 337–359.

Sigman, M., and Dehaene, S. (2005). Parsing a cognitive task: a characterization of the mind's bottleneck. PLoS Biol. *3*, e37, 10.1371/journal.pbio.0030037.

Sleezer, B.J., Castagno, M.D., and Hayden, B.Y. (2016). Rule encoding in orbitofrontal cortex and striatum guides selection. J. Neurosci. *36*, 11223–11237.

Stavisky, S.D., Kao, J.C., Ryu, S.I., and Shenoy, K.V. (2017). Motor cortical visuomotor feedback activity is initially isolated from downstream targets in output-null neural state space dimensions. Neuron *95*, 195–208.e9.

Stephens, D.W., and Anderson, D. (2001). The adaptive value of preference for immediacy: when shortsighted rules have farsighted consequences. Behav. Ecol. *12*, 330–339.

Stephens, D.W., and Krebs, J.R. (1986). Foraging Theory (Princeton University Press).

Stokes, M.G., Kusunoki, M., Sigala, N., Nili, H., Gaffan, D., and Duncan, J. (2013). Dynamic coding for cognitive control in prefrontal cortex. Neuron *78*, 364–375.

Strait, C.E., Blanchard, T.C., and Hayden, B.Y. (2014). Reward value comparison via mutual inhibition in ventromedial prefrontal cortex. Neuron *82*, 1357–1366.

Strait, C.E., Sleezer, B.J., and Hayden, B.Y. (2015). Signatures of value comparison in ventral striatum neurons. PLoS Biol. *13*, e1002173.

Strait, C.E., Sleezer, B.J., Blanchard, T.C., Azab, H., Castagno, M.D., and Hayden, B.Y. (2016). Neuronal selectivity for spatial positions of offers and choices in five reward regions. J. Neurophysiol. *115*, 1098–1111.

Sussillo, D., Churchland, M.M., Kaufman, M.T., and Shenoy, K.V. (2015). A neural network that finds a naturalistic solution for the production of muscle activity. Nat. Neurosci. *18*, 1025–1033.

Tajima, S., Drugowitsch, J., and Pouget, A. (2016). Optimal policy for value-based decision-making. Nat. Commun. *7*, 12400.

Thura, D., and Cisek, P. (2014). Deliberation and commitment in the premotor and primary motor cortex during dynamic decision making. Neuron *81*, 1401–1416.

Thura, D., Beauregard-Racine, J., Fradet, C.-W., and Cisek, P. (2012). Decision making by urgency gating: theory and experimental support. J. Neurophysiol. *108*, 2912–2930.

Wallis, J.D. (2007). Orbitofrontal cortex and its contribution to decision-making. Annu. Rev. Neurosci. *30*, 31–56.

Wang, M.Z., and Hayden, B.Y. (2017). Reactivation of associative structure specific outcome responses during prospective evaluation in reward-based choices. Nat. Commun. *8*, 15821.

Watson, K.K., and Platt, M.L. (2012). Social signals in primate orbitofrontal cortex. Curr. Biol. *22*, 2268–2273.

Wilson, R.C., Takahashi, Y.K., Schoenbaum, G., and Niv, Y. (2014). Orbitofrontal cortex as a cognitive map of task space. Neuron *81*, 267–279.

Wunderlich, K., Rangel, A., and O'Doherty, J.P. (2010). Economic choices can be made using only stimulus values. Proc. Natl. Acad. Sci. USA *107*, 15005–15010.

Xie, Y., Nie, C., and Yang, T. (2018). Covert shift of attention modulates the value encoding in the orbitofrontal cortex. eLife *7*, 1–21.

Yoo, S.B.M., and Hayden, B.Y. (2018). Economic choice as an untangling of options into actions. Neuron *99*, 434–447.

Yoo, S.B.M., Sleezer, B.J., and Hayden, B.Y. (2018b). Robust encoding of spatial information in orbitofrontal cortex and striatum. J. Cogn. Neurosci. *30*, 898–913.

Yoo, S.B.M., Tu, J.C., Piantadosi, S.T., and Hayden, B.Y. (2019). The neural basis of predictive pursuit. bioRxiv. https://doi.org/10.1101/694604.

STAR★METHODS

KEY RESOURCES TABLE

REAGENT or RESOURCE	SOURCE	IDENTIFIER
Deposited Data		
Physiological dataset	collected in the lab	N/A
Experimental Models: Organisms/Strains		
Rhesus macaque (Mucacca mulatta)	California National Primate Research Center Analytical and Resource Core	https://cnprc.ucdavis.edu/research/arc.aspx; RRID:SCR_000696
Software and Algorithms		
MATLAB	The Mathworks, Inc	https://www.mathworks.com/; RRID: SCR_001622
Offline Sorter	Plexon	https://plexon.com/; RRID: SCR_000012
Neuroexplorer	Nex Technologies	https://www.neuroexplorer.com/; RRID: SCR_001818
Brainsight	Rogue Research	https://www.rogue-research.com/tms/brainsight-tms/; RRID:SCR_009539

LEAD CONTACT AND MATERIALS AVAILABILTY

Further information and requests for resource sharing should be directed to and will be fulfilled by the Lead Contact, Seng Bum Michael Yoo (sbyoo.ur.bcs@gmail.com).

EXPERIMENTAL MODEL AND SUBJECT DETAILS

Some of these data were collected expressly for this study (OFC dataset and 24 new cells of the vmPFC datasest) and some were collected earlier but reanalyzed here (the other 156 cells of the vmPFC dataset; Strait et al., 2014). All procedures were approved by the University Committee on Animal Resources at the University of Minnesota (OFC dataset) or at the University of Rochester (both parts of the vmPFC dataset). All procedures were designed and conducted in compliance with the Public Health Service's Guide for the Care and Use of Animals.

Four male rhesus macaques (*Macaca mulatta*, subjects P and S, OFC, and subjects B and J, vmPFC) served as subjects. A small prosthesis for holding the head was used. Animals were habituated to laboratory conditions and then trained to perform oculomotor tasks for liquid reward. A Cilux recording chamber (Crist Instruments) was placed over the prefrontal cortex. Position was verified by magnetic resonance imaging with the aid of a Brainsight system (Rogue Research Inc.). Animals received appropriate analgesics and antibiotics after all procedures. Throughout both behavioral and physiological recording sessions, the chamber was kept sterile with regular antibiotic washes and sealed with sterile caps. All recordings were performed during the animals' light cycle, between 8 AM and 5 PM.

METHOD DETAILS

Electrophysiological techniques, eye tracking, and reward delivery

We approached Areas 13 and 14 through a recording grid (Crist Instruments). We defined these regions according to a standard atlas and recorded broadly from within them. We confirmed recording location before each recording session using our Brainsight system with structural magnetic resonance images taken before the experiment. Neuroimaging was performed at the Rochester Center for Brain Imaging on a Siemens 3T MAGNETOM Trio Tim using 0.5-mm voxels. We confirmed recording locations by listening for characteristic sounds of white and gray matter during recording, which in all cases matched the loci indicated by the Brainsight system.

For the vmPFC recordings, single electrodes (Frederick Haer & Co., impedance range 0.8–4 MU) were lowered using a microdrive (NAN Instruments) until waveforms of between 1 and 3 neuron(s) were isolated. Individual action potentials were isolated on a Plexon system (Plexon, Inc.). Neurons were selected for study solely on the basis of the quality of isolation; we never pre-selected based on task-related response properties.

For the OFC recordings, multicontact electrodes (V-probes, Plexon, Inc) were lowered using the same microdrive system until positioned within the OFC. Following a settling period, all active cells were recorded. Cells were sorted offline by hand by trained electrophysiologists. No automated sorting was used.

Eye position was sampled at 1,000 Hz by an infrared eye-monitoring camera system (SR Research). Stimuli were controlled by a computer running MATLAB (Mathworks) with Psychtoolbox and Eyelink Toolbox. Visual stimuli were colored rectangles on a computer monitor placed 57 cm from the animal and centered on its eyes. A standard solenoid valve controlled the duration of juice delivery. The relationship between solenoid open time and juice volume was established and confirmed before, during, and after recording.

Behavioral task

Subjects performed a two-option gambling task identical to the one we used in a previous investigation (Figure 1; Strait et al., 2014). Two offers were presented on each trial. Each offer was represented by a rectangle 300 pixels tall and 80 pixels wide (11.35° of visual angle tall and 4.08° of visual angle wide). Options offered either a gamble or a safe (100% probability) bet for liquid reward. Gamble offers were defined by both reward size and probability, which were selected with uniform probabilities and independently of one another for each offer and for each trial. Each gamble rectangle had two sections, one red and the other either blue or green. The size of the blue or green portions indicated the probability of winning a medium (165 μL) or large reward (240 μL), respectively (Figure 1). These probabilities were drawn from a uniform distribution between 0% and 100%. Safe offers (1 out of every 8 offers) were entirely gray, and selecting one would result in a small reward (125 μL) 100% of the time.

Offers were separated from the central fixation point by 550 pixels (27.53° of visual angle). The sides of the first and second offer (left or right) were randomized each trial. Each offer appeared for 400 ms followed by a 600 ms empty screen. After the offers were presented one at a time, a central fixation point appeared, and the monkey fixated on it for 100 ms. Then both offers appeared simultaneously and the animal indicated its choice by shifting gaze to its preferred offer, maintaining fixation on it for 200 ms. Failure to maintain gaze for 200 ms would return the monkey to a choice state. Thus, subjects were in theory free to change their mind if they did so within 200 ms (although they seldom did). Following a successful 200-ms fixation, the gamble was immediately resolved and a liquid reward was delivered. Trials that took more than 7 s were considered inattentive and were excluded from analysis (this removed < 1% of trials). Outcomes that yielded rewards were accompanied by a white circle in the center of the chosen offer (see Figure 1B). Each trial was followed by an 800-ms inter-trial interval (ITI) with a blank screen.

Probabilities were drawn from uniform distributions with resolution only limited by the size of the screen's pixels, which let us present hundreds of unique gambles. Offer reward sizes were selected at random and independent of one another with a 43.75% probability of blue (medium reward) gamble, a 43.75% probability of green (large reward) gambles, and 12.5% probability of safe offers. Note that this means two offers with the same reward size could be (and often were) presented in the same trial.

Previous training history for these subjects included a foraging task (Blanchard and Hayden, 2014; see also Calhoun and Hayden, 2015), an attention task (similar to the one used in Hayden and Gallant, 2013), and several reward-based decision tasks (Sleezer et al., 2016; Wang and Hayden, 2017; Pirrone et al., 2018; Heilbronner and Hayden, 2016b).

Data preprocessing

We followed the two pre-processing steps used by Elsayed and colleagues (Elsayed et al., 2016). First, neural responses for each neuron were soft-normalized such that neurons with strong responses had approximately unity firing rate range (normalization factor firing rate range + 20% of maximum firing rate). Second, the neural responses for each neuron were mean-centered at each time as follows: we calculated the mean activity across all conditions of each neuron at each time point and subtracted this mean activity from each condition's response. This process is similar to z-scoring, although it does not implement a full range normalization.

Epoch preference index

The goal of the epoch preference index calculation was to identify the relative weight of each of the two epochs in driving responses of each neuron. We therefore estimated this scalar parameter for each neuron independently. For each neuron, we examined firing within epochs 1 and 2 separately, and within each epoch calculated the range, then divided by the mean firing rate of neuron *i* across whole time over that trial. Because each epoch can have different average magnitude overall, the range was normalized by the the mean firing rate across all neurons (U_{epoch1} or U_{epoch2}). The epoch preference index was then calculated by:

$$EPI(i) = \frac{S_{epoch1}(i)}{\overline{S}_{epoch1}} - \frac{S_{epoch2}(i)}{\overline{S}_{epoch2}}$$

A positive value for this index indicates the neuron is more effectively driven by information in epoch 1 than in epoch 2; a negative value indicates the reverse. Crucially, a bimodal distribution of epoch preference indices indicates that the neurons come from two discrete populations.

Pairwise cross-condition correlation

A central goal of this study was to understand the change in covariance structure across epochs. To do so, we had to generate a within-epoch covariance matrix This matrix $P \in R^{NxCT}$ matrix for neural activity, where N is the total number of neurons, C is the number of conditions (expected value divided into 7 quantile) and T is the number of time points (400 ms length with 10 ms bins, thus, T = 40) in each epoch. Both epochs therefore take the same number of data points. Then the pairwise correlation between all pairs

of neurons are calculated. To visualize the covariance matrices (Figure 2), we clustered pairwise correlation among neurons in epoch 1 by decision-tree method (MATLAB built-in function 'cluster').

Significance test for epoch comparison

To estimate how much correlation there should be between epochs at chance level, we performed a cross-validation procedure. Specifically, we took all trials for offer 1 and randomly divided them into two equal subsets and computed the correlation between the pairwise correlation matrix. This procedure produces a randomized pseudocorrelation on a within-sample measure. We then compared this randomized pseudocorrelation with the true correlation estimated using the same random splits in trials, but this time going across epochs rather than within epochs. We then repeated this process 1000 times produces a range of possible pseudocorrelation values. The mean of this distribution gives an estimate of the correlation that would be observed by chance assuming that all variance across epochs is due to noise: a high value indicates that most of the variance across epochs is explainable by noise and a low value indicates that most of the variance across epochs is explainable by signal. Moreover, the position of the true correlation in this range then can give an estimate of the p value.

The evidence accumulation model

We developed a simple evidence accumulation model incorporating two separate epochs in the following way (Philiastides et al., 2006):

$$x_i(t) = g\int_0^t E_i(\tau)d\tau$$

where x_i(t) is a putative neural variable diffusing over the decision space, g is a gain factor (which we set as 1) and E_t(t) is the instantaneous time-varying amount of evidence. The parameter E_i(t) is defined to have Gaussian distribution, where the mean is given by the strength of tuning for individual neurons(s) and the expected value of offer EV_n, where n indicates the epoch. The activity at each instantaneous time-varying amount of evidence can be expressed as follows:

$$\mu_n = s \times EV_n$$

$$E_i(t) = N(\mu_n, \sigma)$$

in which σ is a standard deviation in variability of drift within trial, which is assumed to be fixed across the epoch of consideration. Since our goal is not to find the exact parameters of the model but to examine the potential for subspace reorganization in an accumulation model, we fixed all the parameters except the correlation of neural tuning strength between offer 1 and offer 2, which is an intrinsic property of each neuron. The varied parameters are the ones that could potentially change the covariance structure of each epoch.

The correlation of tuning between offer 1 and offer 2 is generated in the following way. Initially, we generated tuning strength of each epoch from Gaussian distribution with 0 mean and fixed variance. The correlation matrix ζ was written as

$$\zeta = \begin{pmatrix} 1 & \gamma \\ \gamma & 1 \end{pmatrix}$$

In which γ determines degree of correlation between the tuning strength of two epoch. Then we obtained Cholesky decomposition on correlation matrix and multiplied upper triangle to matrix that contains the tuning strength for each epoch at each column.

Subspace overlap analysis

To estimate the amount of overlap between subspaces for the two epochs, we performed a special analysis. We first performed principal components analysis (PCA) on the matrix P1 for each epoch (see above) to obtain the epoch 1 PCs (we chose the top ten PCs). Thus, each PC is an orthogonal direction in N-dimensional neural space. We obtained the top ten epoch 2 PCs by performing PCA on matrix P2. To examine the relationship between the subspaces, we projected the epoch 1 activity onto the epoch 2 PCs and quantified the percent of variance explained relative to the total variance of epoch 1. (We also did the reverse, mutatis mutandis. We then defined the alignment index (A) as the ratio between overall variance in epoch 1 by top ten PCs and amount of variance of epoch 1 captured by epoch 2 PC space, which can be written as:

$$A_{idx} = \frac{Tr\left(D_{epoch2}^T C_{epoch1} D_{epoch2}\right)}{\sum_{i=1}^{sel\_dim} \sigma_{epoch1}(i)}$$

where D_{epoch2} is the set of top10 eigenvectors obtained by PCA. The term C_{epoch1} is the covariance of the matrix of epoch 1 (P1). The term $^{\sigma}epoch1^{(i)}$ is the i-th singular value of C_{epoch1}. The term Tr() is the matrix trace which sums along the diagonal entry. In this equation, the quantity found in the denominator serves to normalize the alignment index by the sum of the variance from top 10 dimension

of the epoch 1 data. As a result, the alignment index ranges from 0 to 1, which 0 indicates perfect orthogonality and 1 indicates perfect alignment.

Invariant encoding model

The coding model posits that there is one neuron that has a dedicated invariant tuning function between offer 1 and offer 2. The neural responses during offer presentation were a function of the reward amount and probability of presented offer. We also included side of offer since core economic regions are sensitive to positional information (Strait et al., 2016; Yoo et al., 2018). The relative sensitivity is determined by beta value obtained by general linear model like previous study (Strait et al., 2014).

Advanced method for demonstrating fully orthogonal subspace

To identify the most orthogonal epoch 1 and epoch 2 subspaces, we applied a method that maximizes the sum of the variance of each epoch's responses in each epoch's subspace, which is by maximizing $Tr(Q^T_{epoch\_nth} C_{epoch\_nth} Q_{epoch\_nth})$ where C_{epoch_nth} is the covariance matrix of nth epoch and Q_{epoch1} is the eigenvector of nth epoch subspace. This term reflects the variance captured nth epoch. The critical component of this procedure is constructing the cost function by:

$$\left|Q_{epoch1}, Q_{epoch2}\right| = \text{argmax}_{\left|Q_{epoch1}, Q_{epoch2}\right|} \left(\frac{Tr\left(Q^T_{epoch1} C_{epoch1} Q_{epoch1}\right)}{\sum_{i=1}^{sel\_dim} \sigma_{epoch1}(i)} + \frac{Tr\left(Q^T_{epoch1} 2C_{epoch2} Q_{epoch2}\right)}{\sum_{i=1}^{sel\_dim} \sigma_{epoch2}(i)} \right)$$

Where ${}^{\sigma}epoch1^{(i)}$ is the i-th singular value of C_{epoch1} and ${}^{\sigma}epoch2^{(i)}$ is the i-th singular value of Ce_{poch2}. Then, the manifold is jointly optimized. We chose the dimensionality of Q_{epoch1} to match the number of epoch1 PCs that capture ~80% of variance ($d_{epoch1} = 5$). We selected Q_{epoch2} with same procedure ($d_{epoch2} = 5$).

Computationally, we employed the manifold optimization toolbox (Boumal et al., 2014). We optimized the objective function based on particle swarm and a nonlinear Grasmann manifold was selected. This method simultaneously identifies the subspaces, while constraining them to be completely orthogonal (Cunningham and Ghahramani, 2014; Elsayed et al., 2016). In addition, the optimization objective is suitably normalized by the singular values in the denominators. Thus, it is insensitive to the relative dimensionality and amount of variance explained by the two subspaces.

Analytical technique demonstrating linked relationship between the epoch

To investigate the relation between neural activity in the two subspaces, we projected the population activity for all conditions in epoch 1 onto the epoch 1 subspace and, separately, projected the epoch 2 activity onto the epoch 2 subspace. The subspace are constructed by optimizing cost function discussed in the section above. $X_{epoch1} \in R^{5xC}$ is the matrix that contains the activity projected onto the epoch 1 subspace at the end of epoch 1 (300 ms after offer 1 onset, lasting 50 ms). $X_{epoch2} \in R^{5xC}$ is the matrix that contains the activity projected onto the epoch 2 subspace at the middle of the epoch 2 (200 ms after epoch 2 onset). We used the same timings for vmPFC and OFC. To investigate the relation between X_{epoch1} and X_{epoch2}, we solved the linear equation as follows with Moore-Penrose pseudoinverse (MATLAB function pinv): $X_{epoch1} \approx WX_{epoch2}$. Thus $W \in R^{5x5}$ is a matrix of regression weights that links the epoch 1 and epoch 2 responses. Then, we quantified the quality of the fit of this decoder by calculating:

$$R^2 = 1 - \frac{\|X_{epoch2} - WX_{epoch1}\|_F^2}{\|X_{epoch2}\|_F^2}$$

We additionally quantified the generalization performance of the linear decoder by performing leave-one-out cross-validation and measuring R^2 for test conditions that were not used to fit the decoder. The data R^2 were compared with a control distribution of R^2-values obtained by shuffling each row of X_{epoch1} independently and fitting the same linear decoder to predict X_{epoch2}.

DATA AND CODE AVAILABILITY

The part of the datasets generated during the current study are available on the Github (https://github.com/sbyoo/subreorg/). Full data that support the findings of this study are available from the corresponding author upon reasonable request. The code is available at the Github repository of the corresponding author (https://github.com/sbyoo/subreorg/).